JOURNAL OF AIRCRAFT
Vol. 29, No. 5, Sept.–Oct. 1992

Nine-Degree-of-Freedom Simulation of Rotating Parachute Systems

Karl-Friedrich Doherr*
DLR-Institut für Flugmechanik, 3300 Braunschweig, Germany
and
Hartmut Schilling†
Rheinmetall GmbH, 4000 Düsseldorf, Germany

Rotating parachutes are used, for example, to decelerate and spin the submunitions of defense weapons against armored ground vehicles. Usually, the desired system performance data, like velocity of descent, rate of spin, submunition inclination angle against vertical, and dynamic stability are so difficult to meet all at the same time that intensive design and redesign work is necessary until an optimal parachute-load configuration is found. To limit time-consuming field tests with expensive hardware, a 9-degree-of-freedom (DOF) computer program was developed for the simulation of the trajectory and the dynamic behavior of the parachute system. Now the influence of the important system parameters can be analysed in a simulation first. In this article the mathematical model of the parachute-load system is presented together with typical simulation results.

Nomenclature

C^{kl}	=	transformation matrix from $x_i^{(l)}$ to $x_i^{(k)}$ coordinates
C_D, C_L, C_N, C_T	=	force coefficients
C_l, C_m	=	moment coefficients
C_{lo}	=	C_l at $p = \Omega_1 = 0$
C_{lp}, $C_{N\alpha}$	=	aerodynamic derivatives
D	=	drag
d	=	reference diameter
e_1, e_2, e_3,	=	unit vectors of the axes x_1, x_2, x_3
F	=	force vector
g	=	gravitational acceleration vector
I	=	moment of inertia tensor
I_x, I_y, I_z	=	axial moments of inertia
L	=	lift
L	=	rolling moment
ℓ_R	=	vector from connection point O to the center of pressure
ℓ_S	=	vector from connection point O to the center of gravity
M	=	moment vector
M	=	pitching moment
m	=	mass
N	=	normal force
Q	=	quaternion
q_0, q_1, q_2, q_3	=	quaternion elements
r_O	=	vector from earth-fixed point E to the connection point O
T	=	tangential force
V	=	velocity vector
x, y, z	=	orthogonal coordinates
$x_i^{(k)}$	=	auxiliary coordinates, $i = 1, 2, 3$; $k = 1, \ldots, 6$
Z	=	state vector
α	=	angle of attack
α_{stab}	=	angle at which $C_{N\alpha}$ becomes positive
Ω	=	angular velocity vector
Ψ, Θ, Φ	=	Euler angles
ρ	=	air density

Subscripts

E, L, P	=	earth, load, parachute
O	=	parachute connection point
1, 2, 3	=	x, y, z direction

Superscripts

0, 1, 2, 3, 4, 5, 6	=	number of Euler angle rotations

I. Introduction

FOR many applications parachute-load systems can be treated as single rigid masses. It is sufficient when, for example, only the trajectory of the center of gravity is to be simulated. But, it fails when the relative motion between the parachute and the load needs to be considered, as in the case of rotating parachutes with stores that can pitch up. Then two coupled masses must be taken into account. Assuming that the two masses are connected by a joint, this leads to a mathematical model with 9 DOF.

In 1968 Wolf[1] was the first to publish a nonrigid parachute and payload model. His paper stimulated dynamic wind tunnel experiments conducted by Doherr[2,3] with 5 DOF, where both the load and the parachute were free to pitch and yaw. Additionally the parachute could perform a rolling motion. In 1984 Pillasch et al.[4] introduced the Lagragian equations of motion of a coupled three-body parachute submunition system with up to 15 DOF, including a friction plate and elastic suspension lines.

The present paper is an extension of Doherr's Ph.D. thesis[3] to rotating and nonrotating parachute systems in free-flight with 6 DOF for the load (position and attitude) and up to 3 DOF for the parachute. Depending on the design of the joint the parachute may yaw and/or pitch and/or roll with respect to the load. Friction in the joint and elasticity of the suspension lines are neglected. The corresponding 9-DOF

Received Feb. 16, 1991; presented as Paper 91-0877 at the AIAA 11th Aerodynamic Decelerator Systems Technology Conference, San Diego, CA, April 9–11, 1991; revision received Aug. 5, 1991; accepted for publication Aug. 20, 1991.

*Dr.-Ing., M. Sc., Head, Mathematical Methods and Data Handling Branch. Member AIAA.

†Dr. rer. nat. habil., Head, System Simulation Department. Member AIAA.

mathematical model, based on Euler's equations of motion, was presented by Doherr and Saliaris[5] during a lecture series in 1987. Paus[6] developed the strategy for the numerical solution of the coupled nonlinear differential equations of motion by Runge-Kutta algorithms.

Since that time the simulation program has been developed, tested, and used to investigate, for example, the influence of the parachute aerodynamics on pitch angle and angular rate of rotating submunitions.

II. Mathematical Model

A. Simplifying Assumptions

1) The load L and the parachute P are both rigid bodies, connected in an arbitrary point O located in the load (Fig. 1).

2) Depending on the design of the joint the parachute is either rigidly attached or may yaw and/or pitch and/or roll relative to the load.

3) The Earth E is considered to be flat, nonrotating, and fixed in space; the Earth-fixed reference system is an inertial system.

B. Coordinate Systems and Transformations

The following coordinate systems (Figs. 1 and 2) are used 1) Earth-fixed (space-fixed) x_E, y_E, z_E, with origin E; 2) load-fixed x_L, y_L, z_L, with origin O; 3) parachute-fixed x_P, y_P, z_P, with origin O; and 4) auxiliary ($k = 0, 1, \ldots, 6$) $x_1^{(k)}, x_2^{(k)}, x_3^{(k)}$, with origin E.

The auxiliary coordinate systems are introduced to describe the attitudes of the body-fixed coordinate systems after $k = 0$–6 Euler angle rotations through $\Psi_L, \Theta_L, \Phi_L, \Psi_P, \Theta_P, \Phi_P$. Initially the auxiliary coordinates, $x_1^{(0)}, x_2^{(0)}, x_3^{(0)}$, are parallel to the earth-fixed coordinates x_E, y_E, z_E (Fig. 2). By the first rotation about the axis $x_3^{(0)}$ through Ψ_L the auxiliary coordinates are turned into the position $x_i^{(1)}$, $i = 1, 2, 3$. The upper index indicates the number of rotations. After two more rotations about $x_2^{(1)}$ through Θ_L and about $x_1^{(2)}$ through Φ_L the auxiliary coordinates become parallel to the load-fixed coordinates x_L, y_L, z_L. Then, after three more equivalent rotations through Ψ_P, Θ_P, and Φ_P they become parallel to the parachute-fixed coordinates x_P, y_P, z_P.

The components of a vector V in two differently oriented coordinate systems, for example $x_i^{(6)}$ and $x_i^{(3)}$, are identified by the upper index

$$V^{(3)} = V^{(6)} \cdot C^{63}; \qquad V^{(6)} = C^{63} \cdot V^{(3)} \tag{1a}$$

or, in components, for $i = 1, 2, 3$

$$V_i^{(3)} = \sum_{n=1}^{3} V_n^{(6)} C_{ni}^{63}; \qquad V_i^{(6)} = \sum_{n=1}^{3} C_{in}^{63} V_n^{(3)} \tag{1b}$$

Both sets of components are related by the corresponding transformation matrix, in this case C^{63}

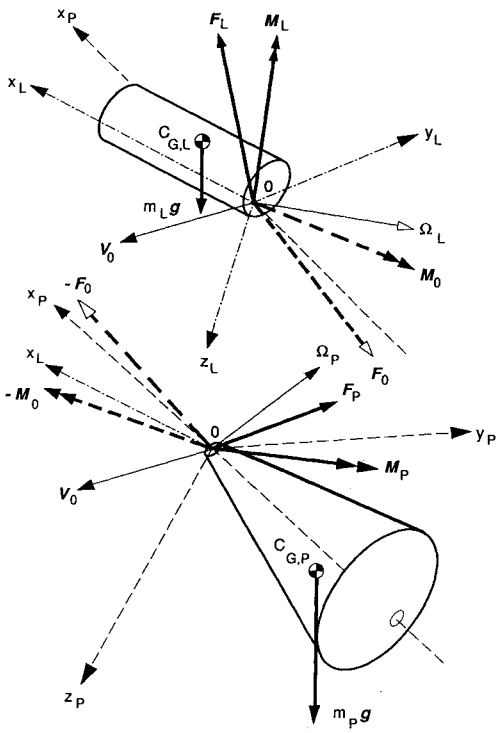

Fig. 1 Parachute-load system.

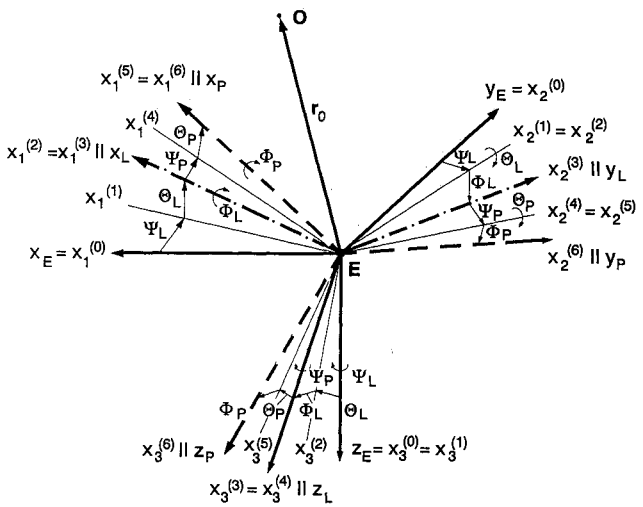

Fig. 2 Coordinates and Euler angles.

C. Kinematic Variables and State Vector

The position of the parachute system is given by the vector r_o from the earth-fixed origin E to the parachute connection point O (Figs. 1 and 2). The attitude of the load is described relative to the earth by the Euler angles Ψ_L, Θ_L, Φ_L (in the order of rotation). The attitude of the parachute is described relative to the load by three more Euler angles Ψ_P, Θ_P, Φ_P.

The motion of the system is expressed by the translatory velocity V_O and by the angular velocities of the load, Ω_L, and

$$C^{63} = \begin{bmatrix} \cos\Theta_P \cos\Psi_P & \cos\Theta_P \sin\Psi_P & -\sin\Theta_P \\ \sin\Phi_P \sin\Theta_P \cos\Psi_P - \cos\Phi_P \sin\Psi_P & -\sin\Phi_P \sin\Theta_P \sin\Psi_P + \cos\Phi_P \cos\Psi_P & \sin\Phi_P \cos\Theta_P \\ \cos\Phi_P \sin\Theta_P \cos\Psi_P + \sin\Phi_P \sin\Psi_P & \cos\Phi_P \sin\Theta_P \sin\Psi_P - \sin\Phi_P \cos\Psi_P & \cos\Phi_P \cos\Theta_P \end{bmatrix} \tag{2}$$

of the parachute, $\boldsymbol{\Omega}_P$, relative to earth-fixed coordinates. This leads to 18 independent kinematic variables corresponding to the 9 DOF of the system.

To avoid a singularity, which exists in the Euler angle differential equations at $\Theta_L = \pm 90$ deg, the Euler angles of the load are replaced by the four elements q_0, q_1, q_2, q_3 of the quaternion Q, which are related by the norm

$$q_0^2 + q_1^2 + q_2^2 + q_3^2 = 1 \tag{3}$$

Then, the state vector $\boldsymbol{Z}$ has 19 elements

$$\boldsymbol{Z} = (r_{O1}, r_{O2}, r_{O3}, q_0, q_1, q_2, q_3, \Psi_P, \Theta_P, \Phi_P, V_{O1}, V_{O2}, V_{O3}, \Omega_{L1}, \Omega_{L2}, \Omega_{L3}, \Omega_{P1}, \Omega_{P2}, \Omega_{P3})^T \tag{4}$$

The corresponding 19 different equations are derived in the following.

D. Trajectory of the Connection Point *O*

The projection of the velocity vector V_o on earth-parallel coordinates provides three differential equations for the trajectory of the point O

$$\dot{\boldsymbol{r}}_O^{(0)} = \boldsymbol{V}_O^{(0)} = \boldsymbol{V}_O^{(6)} \cdot \boldsymbol{C}^{60} = \boldsymbol{V}_O^{(6)} \cdot \boldsymbol{C}^{63} \cdot \boldsymbol{C}^{30} \tag{5}$$

$\boldsymbol{C}^{30}$ follows from $\boldsymbol{C}^{63}$ by replacing Ψ_P, Θ_P, and Φ_P in Eq. (2) by Ψ_L, Θ_L, and Φ_L.

E. Load Euler Angles and Quaternions

The Euler angles are related to the quaternion elements by[7]

$$\begin{aligned}
q_0 &= +\cos\frac{\Phi_L}{2}\cos\frac{\Theta_L}{2}\cos\frac{\Psi_L}{2} + \sin\frac{\Phi_L}{2}\sin\frac{\Theta_L}{2}\sin\frac{\Psi_L}{2} \\
q_1 &= +\cos\frac{\Phi_L}{2}\sin\frac{\Theta_L}{2}\sin\frac{\Psi_L}{2} - \sin\frac{\Phi_L}{2}\cos\frac{\Theta_L}{2}\cos\frac{\Psi_L}{2} \\
q_2 &= -\cos\frac{\Phi_L}{2}\sin\frac{\Theta_L}{2}\cos\frac{\Psi_L}{2} - \sin\frac{\Phi_L}{2}\cos\frac{\Theta_L}{2}\sin\frac{\Psi_L}{2} \\
q_3 &= -\cos\frac{\Phi_L}{2}\cos\frac{\Theta_L}{2}\sin\frac{\Psi_L}{2} + \sin\frac{\Phi_L}{2}\sin\frac{\Theta_L}{2}\cos\frac{\Psi_L}{2}
\end{aligned} \tag{6}$$

with linear differential equations which are free of singularities

$$\begin{aligned}
\dot{q}_0 &= 0.5(+q_1\Omega_{L1} + q_2\Omega_{L2} + q_3\Omega_{L3}) \\
\dot{q}_1 &= 0.5(-q_0\Omega_{L1} - q_3\Omega_{L2} + q_2\Omega_{L3}) \\
\dot{q}_2 &= 0.5(+q_3\Omega_{L1} + q_0\Omega_{L2} - q_1\Omega_{L3}) \\
\dot{q}_3 &= 0.5(-q_2\Omega_{L1} + q_1\Omega_{L2} - q_0\Omega_{L3})
\end{aligned} \tag{7}$$

After integrating Eq. (7), the elements of $\boldsymbol{C}^{30}$ can be calculated from

$$\boldsymbol{C}^{30} = \begin{pmatrix} q_0^2 + q_1^2 - q_2^2 - q_3^2 & 2(q_1q_2 - q_0q_3) & 2(q_1q_3 + q_0q_2) \\ 2(q_1q_2 + q_0q_3) & q_0^2 - q_1^2 + q_2^2 - q_3^2 & 2(q_2q_3 - q_0q_1) \\ 2(q_1q_3 - q_0q_2) & 2(q_2q_3 + q_0q_1) & q_0^2 - q_1^2 - q_2^2 + q_3^2 \end{pmatrix} \tag{8}$$

During the simulation, the Euler angles of the load are needed explicitly only once, namely to compute the initial values of $q_i(t_0)$ from Eq. (6) with $\Psi_L(t_0)$, $\Theta_L(t_0)$, $\Phi_L(t_0)$. For the next and all following steps it is sufficient to work only with the transformation matrix. If desired, the Euler angles can be calculated from

$$\tan\Psi_L = C_{12}^{30}/C_{11}^{30};\ \tan\Phi_L = C_{23}^{30}/C_{33}^{30};\ \sin\Theta_L = -C_{13}^{30} \tag{9}$$

F. Parachute Euler Angles

The angular velocity of the parachute differs from the angular velocity of the load by the relative rate of rotation between both bodies. This can be expressed by the Euler angle rates[3]

$$\begin{aligned}
\dot{\Psi}_P &= \frac{1}{\cos\Theta_P}(\Omega_{P2}\sin\Phi_P + \Omega_{P3}\cos\Phi_P) \\
&\quad - (\Omega_{L1}\cos\Psi_P\tan\Theta_P + \Omega_{L2}\sin\Psi_P\tan\Theta_P + \Omega_{L3}) \\
\dot{\Theta}_P &= \Omega_{P2}\cos\Phi_P - \Omega_{P3}\sin\Phi_P \\
&\quad + \Omega_{L1}\sin\Psi_P - \Omega_{L2}\cos\Psi_P \\
\dot{\Phi}_P &= \Omega_{P1} + (\Omega_{P2}\sin\Phi_P + \Omega_{P3}\cos\Phi_P)\tan\Theta_P \\
&\quad - (\Omega_{L1}\cos\Psi_P + \Omega_{L2}\sin\Psi_P)\frac{1}{\cos\Theta_P}
\end{aligned} \tag{10}$$

In its general form, Eq. (10) is derived for the case that the parachute is allowed to rotate about all its three axes. The cases of restricted degrees of rotational freedom are discussed later.

For the parachute canopy, as distinct from the load, the Euler angle differential equations are not substituted by the corresponding quaternion algorithm, because a relative pitch angle of 90 deg between the parachute and the load is not a case of practical interest.

G. Equations of Motion

Six more differential equations are derived from the equations of motion, based on the equilibrium of forces and moments, which act on the parachute-load system (Fig. 1). As reference point the connection point O has been selected instead of the center of gravity of the system.[3] This approach is not common in dynamics, but it avoids additional variables which would otherwise have to be introduced.

Equilibrium of forces

$$\begin{aligned}
&m_L\frac{\mathrm{d}}{\mathrm{d}t}[V_0 + \boldsymbol{\Omega}_L \times \boldsymbol{\ell}_{SL}] + m_P\frac{\mathrm{d}}{\mathrm{d}t}[V_0 + \boldsymbol{\Omega}_P \times \boldsymbol{\ell}_{SP}] \\
&\quad = (m_L + m_P)\boldsymbol{g} + \boldsymbol{F}_L + \boldsymbol{F}_P
\end{aligned} \tag{11}$$

Equilibrium of moments about O

$$\begin{aligned}
&\frac{\mathrm{d}}{\mathrm{d}t}[\boldsymbol{I}_L(0)\cdot\boldsymbol{\Omega}_L + m_L\boldsymbol{\ell}_{SL} \times \frac{\mathrm{d}}{\mathrm{d}t}V_0 + \frac{\mathrm{d}}{\mathrm{d}t}[\boldsymbol{I}_P(0)\cdot\boldsymbol{\Omega}_P] \\
&\quad + m_P\boldsymbol{\ell}_{SP} \times \frac{\mathrm{d}}{\mathrm{d}t}V_0 = \boldsymbol{\ell}_{SL} \times m_L\boldsymbol{g} + \boldsymbol{\ell}_{SP} \times m_P\boldsymbol{g} \\
&\quad + \boldsymbol{M}_L + \boldsymbol{M}_P
\end{aligned} \tag{12}$$

For the numerical solution Eqs. (11) and (12) are projected on the rotating parachute-parallel coordinates $x_i^{(6)}$

$$(m_L + m_P)(\dot{V}_0 + \boldsymbol{\Omega}_P \times \boldsymbol{V}_0)^{(6)} + m_L \boldsymbol{C}^{63} \cdot [\dot{\boldsymbol{\Omega}}_L \times \boldsymbol{\ell}_{SL} + \boldsymbol{\Omega}_L \times (\boldsymbol{\Omega}_L \times \boldsymbol{\ell}_{SL})]^{(3)} + m_P[\dot{\boldsymbol{\Omega}}_P \times \boldsymbol{\ell}_{SP} + \boldsymbol{\Omega}_P \times (\boldsymbol{\Omega}_P \times \boldsymbol{\ell}_{SP})]^{(6)} = \boldsymbol{C}^{63} \cdot \boldsymbol{F}_L^{(3)} + \boldsymbol{F}_P^{(6)} + (m_L + m_P)\boldsymbol{C}^{60} \cdot \boldsymbol{g}^{(0)} \tag{13}$$

and

$$\boldsymbol{C}^{63} \cdot [\boldsymbol{I}_L(0) \cdot \dot{\boldsymbol{\Omega}}_L + \boldsymbol{\Omega}_L \times (\boldsymbol{I}_L(0) \cdot \boldsymbol{\Omega}_L)]^{(3)} + m_L(\boldsymbol{C}^{63} \cdot \boldsymbol{\ell}_{SL}^{(3)}) \times (\dot{\boldsymbol{V}}_0 + \boldsymbol{\Omega}_P \times \boldsymbol{V}_0)^{(6)} + [\boldsymbol{I}_P(0) \cdot \dot{\boldsymbol{\Omega}}_P + \boldsymbol{\Omega}_P \times (\boldsymbol{I}_P(0) \cdot \boldsymbol{\Omega}_P)]^{(6)} + m_P \boldsymbol{\ell}_{SP}^{(6)} \times (\dot{\boldsymbol{V}}_0 + \boldsymbol{\Omega}_P \times \boldsymbol{V}_0)^{(6)} = \boldsymbol{C}^{63} \cdot [\boldsymbol{M}_L + \boldsymbol{\ell}_{SL} \times m_L(\boldsymbol{C}^{30} \cdot \boldsymbol{g}^{(0)})]^{(3)} + \boldsymbol{M}_P^{(6)} + \boldsymbol{\ell}_{SP}^{(6)} \times m_P(\boldsymbol{C}^{60} \cdot \boldsymbol{g}^{(0)}) \tag{14}$$

Here the dot implies differentiation with respect to time of the components in rotating coordinates.

H. Coupling Moment in *O*

The remaining three differential equations follow from the coupling moment $\boldsymbol{M}_0$ between the load and the parachute

$$\boldsymbol{M}_0 = \frac{\mathrm{d}}{\mathrm{d}t}[\boldsymbol{I}_L(0) \cdot \boldsymbol{\Omega}_L] + m_L \boldsymbol{\ell}_{SL} \times \frac{\mathrm{d}}{\mathrm{d}t} \boldsymbol{V}_0 - \boldsymbol{\ell}_{SL} \times m_L \boldsymbol{g} - \boldsymbol{M}_L \tag{15}$$

or, in load-parallel coordinates

$$\boldsymbol{M}_0^{(3)} = [\boldsymbol{I}_L(0) \cdot \dot{\boldsymbol{\Omega}}_L + \boldsymbol{\Omega}_L \times (\boldsymbol{I}_L(0) \cdot \boldsymbol{\Omega}_L)]^{(3)} + m_L \boldsymbol{\ell}_{SL}^{(3)} \times [(\dot{\boldsymbol{V}}_0 + \boldsymbol{\Omega}_P \times \boldsymbol{V}_0)^{(6)} \cdot \boldsymbol{C}^{63}] - m_L \boldsymbol{\ell}_{SL}^{(3)} \times (\boldsymbol{C}^{30} \cdot \boldsymbol{g}^{(0)}) - \boldsymbol{M}_L^{(3)} \tag{16}$$

In this analysis, friction between the load and the parachute is neglected. When the parachute is allowed to rotate about an axis relative to the load, no moment about this axis is transferred or, in other words, the component of the coupling moment parallel to this axis is zero.

Therefore, the coupling conditions are

$$\Psi_P \begin{cases} = 0, M_{O3}^{(3)} \neq 0; \\ \neq 0, M_{O3}^{(3)} = 0 \end{cases} \quad \Theta_P \begin{cases} = 0, M_{O2}^{(4)} \neq 0; \\ \neq 0, M_{O2}^{(4)} = 0 \end{cases} \quad \Phi_P \begin{cases} = 0, M_{O1}^{(5)} \neq 0 \\ \neq 0, M_{O1}^{(5)} = 0 \end{cases} \tag{17}$$

For each non-zero parachute Euler angle, one differential equation can be derived from Eq. (10) and another one from Eqs. (16) and (17). However, if an Euler angle is selected to be zero, the DOF are reduced by one and the number of necessary kinematic variables and differential equations are reduced by two. In that case Eqs. (15) and (17) can be used to determine the corresponding component of the coupling moment.

I. Aerodynamic Forces and Moments

The aerodynamic forces and moments are modelled in the usual way by coefficients[3,8]

$$N = C_N \frac{\rho}{2} V^2 \frac{\pi}{4} \mathrm{d}^2 \quad \text{Normal force}$$

$$T = C_T \frac{\rho}{2} V^2 \frac{\pi}{4} \mathrm{d}^2 \quad \text{Tangential force}$$

$$M = C_m \frac{\rho}{2} V^2 \frac{\pi}{4} \mathrm{d}^3 \quad \text{Pitching moment}$$

$$L = \left(C_{lo} + C_{lp} \frac{\Omega_1 \mathrm{d}}{2V}\right) \frac{\rho}{2} V^2 \frac{\pi}{4} \mathrm{d}^3 \quad \text{Rolling moment} \tag{18}$$

The coefficients are, in general, functions of angle of attack and Mach number and can be either expressed by derivatives or be tabulated.

The apparent mass forces and moments of the parachute are modelled by a 6 × 6 tensor, which has only five non-zero elements in case of a parachute with axial symmetry. For details see Ref. 9. No apparent mass effects are appropriate for the load.

J. Numerical Solution Scheme

The strategy for the numerical solution, set up by Paus,[6] was to bring the differential equations into the state vector form

$$\dot{\boldsymbol{Z}} = A \cdot \boldsymbol{Z} + B \tag{19}$$

which allows numerical integration by standard algorithms like Runge-Kutta-Fehlberg with step size control.

To be able to achieve state vector form, the apparent mass terms were considered to be external forces and moments caused by accelerations and velocities at an earlier time $(t\text{-}\tau)$ as proposed in the water tunnel tests performed by Cockrell et al.[10-12] This way the corresponding terms could be kept on the right side of Eq. (19).

III. Examples

A. System Data

The flights of a cylindrical load with a rotating parachute are simulated as examples. Investigated are the influences of parachute stability, rolling moment, normal force fluctuations, and wind gusts on the dynamic behavior of the system.

At the deployment of the parachute at an altitude of 200 m the load is flying with zero angle of attack on a 60 deg declined trajectory at 70 m/s velocity, spinning at 5 rev/s. Both load and parachute are assumed to possess axial symmetry. The parachute connection point is positioned off the center line of the cylinder so that the load achieves a static inclination angle of about 20 deg against vertical at zero angular rate, while the motion of the parachute relative to the load is restricted to rotation about the Euler angle Ψ_P only. The system data are collected in Table 1.

The aerodynamic coefficients of the cylinder and the parachute are plotted in Figs. 3 and 4. Here, the apparent mass effects of both the load and the parachute have been neglected.

So far, very little aerodynamic data of rotating parachutes have been published. Therefore, two principal cases were investigated:

Case 1—a "stable" parachute that produces mainly drag and negligible lift and is, as shown below, already statically stable at $|\alpha| \geq \alpha_{\text{stab}} = 0$ deg.

Case 2—an "unstable" parachute, which becomes statically stable at $|\alpha| \geq \alpha_{\text{stab}} = 5$ deg.

Tangential and normal force coefficients are related to drag and lift coefficients by

Table 1 System data

			Load	Parachute
Mass	m	kg	11.5	0.35
Vector from 0 to	ℓ_{S1}	m	0.100	−0.6934
center of gravity	ℓ_{S2}	m	−0.035	0
(body-fixed)	ℓ_{S3}	m	0.000	0
Moments of inertia	I_x	kg m²	0.035	0.048
with respect to the	I_y	kg m²	0.050	0.116
centers of gravity;	I_z	kg m²	0.050	0.116
deviation moments	I_{ij}	kg m²	0	0
Reference diameter	d	m	0.15	1.50
Length cylinder	ℓ	m	0.20	—
Length suspension line	ℓ	m	—	0.81
Vector from 0 to	ℓ_{R1}	m	Variable	−0.81
center of pressure	ℓ_{R2}	m	−0.035	0
(body-fixed)	ℓ_{R3}	m	0.0	0
Tangential force coef.	C_T	—	Fig. 3	0.75
Normal force coef.	C_N	—	Fig. 3	Fig. 4
Pitching moment coef.	C_m	—	Fig. 3	$-C_N\ell_R/d$
Pitch damping coef.	C_{mq}	—	Variable	—
Rolling moment coef.	C_{lo}	—	0	Variable
Roll damping deriv.	C_{lp}	—	0	−0.017

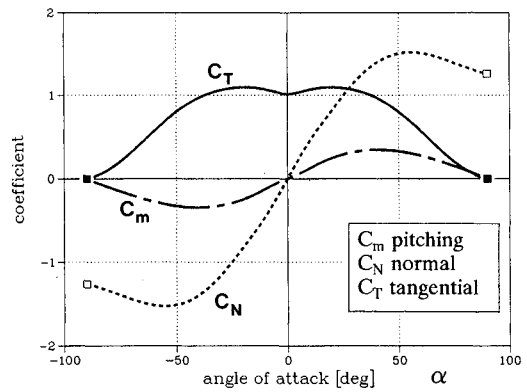

Fig. 3 Aerodynamic coefficients of the cylindrical load.

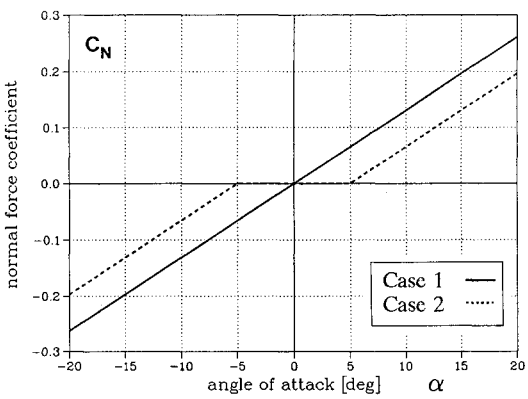

Fig. 4 Parachute normal force coefficients C_N.

$$C_T = C_D \cos\alpha - C_L \sin\alpha$$
$$C_N = C_D \sin\alpha + C_L \cos\alpha \qquad (20)$$

At small angles of attack (i.e., $|\alpha| \leq 6$ deg, $\sin\alpha \approx \alpha$, $\cos\alpha \approx 1$) and negligible lift, the coefficients of the parachute can be approximated by

$$C_T = C_D; \qquad C_N = C_D\alpha; \qquad C_{N\alpha} = C_D \qquad (21)$$

Thus, the case 1 parachute generates already at zero angle of attack a large positive normal force gradient $C_{N\alpha}$, which is the measure of the static stability of parachutes.

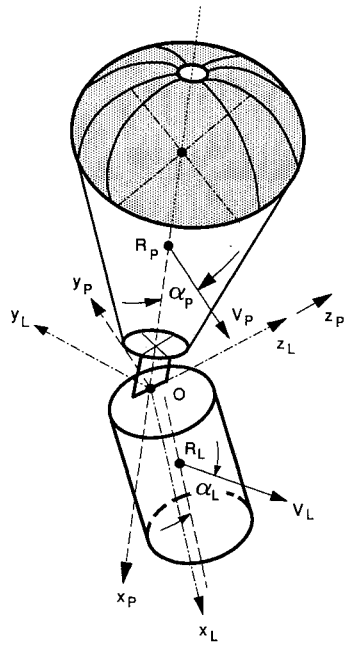

Fig. 5 Effective angles of attack, α_L and α_P.

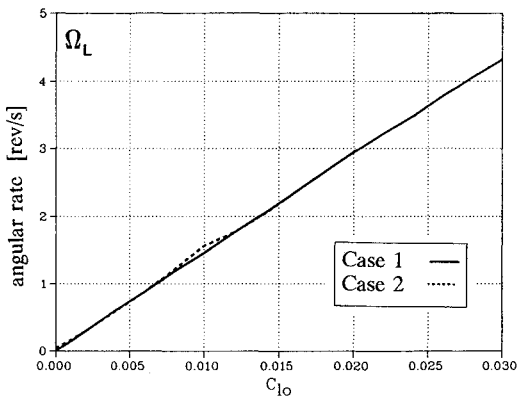

Fig. 6 Submunition angular rate, Ω_L, in steady descent vs parachute rolling moment coefficient, C_{lo}.

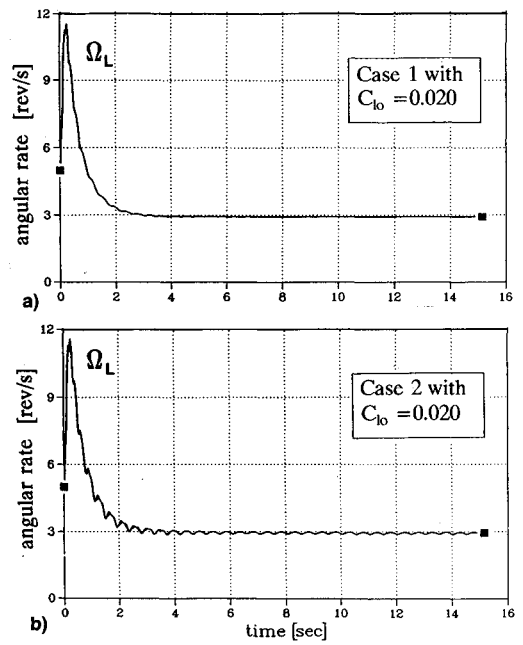

Fig. 7 Submunition angular rate Ω_L vs time, for $C_{lo} = 0.020$: a) case 1 (stable parachute), and b) case 2 (unstable parachute).

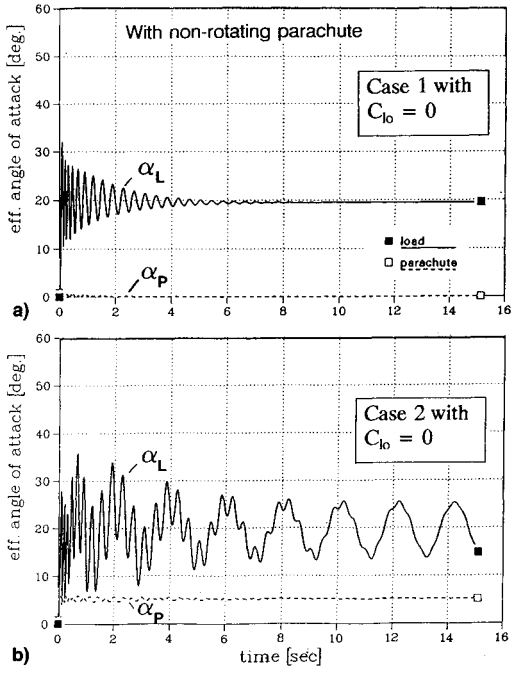

Fig. 8 Effective angles of attack, α_L and α_P, vs time without rotation ($C_{lo} = 0$): a) case 1 (stable parachute), and b) case 2 (unstable parachute).

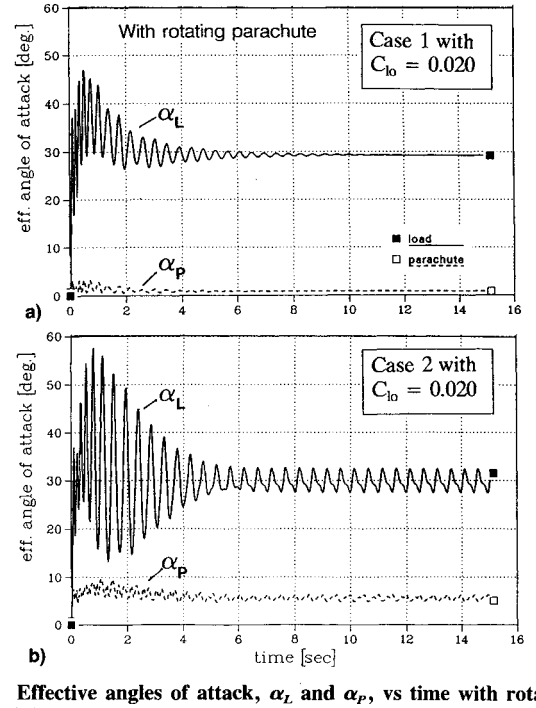

Fig. 9 Effective angles of attack, α_L and α_P, vs time with rotation ($C_{lo} = 0.020$): a) case 1 (stable parachute), and b) case 2 (unstable parachute).

Another parameter of the stability of a parachute is the angle α_{stab} at which $C_{N\alpha}$ becomes positive. In wind tunnel tests, when the parachute is attached at one point only, it oscillates about an angle close to α_{stab}. Thus, α_{stab} can be observed easily and recorded with a camera.

Because of the assumed axial symmetry of the system, the effective angles of attack of the two bodies can be measured in the planes, which are defined by the corresponding longitudinal axes and the velocity vectors at the centers of pressure (Fig. 5):

$$\alpha_L = \arccos \frac{V_{L1}}{V_L}; \qquad \alpha_P = \arccos \frac{V_{P1}}{V_P} \tag{22}$$

B. Angular Rate

For the simulation, Ref. 8 was used for the derivatives of the parachute rolling moment coefficient, C_{lo} and C_{lp}. Then, C_{lo} was varied from 0 to 0.030. For both cases under consideration, the angular rate

$$\Omega_L = \sqrt{\Omega_{L1}^2 + \Omega_{L2}^2 + \Omega_{L3}^2} \tag{23}$$

which the system achieves at steady state, increases almost linearly with C_{lo} (Fig. 6). Rolling moment derivatives of $C_{lo} = 0.020$ and $C_{lp} = -0.017$ produce a steady state angular rate of 3 rev/s (Fig. 7).

C. Effective Angles of Attack

In steady descent the submunition is required to rotate at a constant angular rate with very small pitch, yaw and roll oscillations. These conditions require that the effective angles of attack, α_L and α_P, which are easier to interpret than the Euler angles, also vary very little with time.

In case 1, with the stable parachute, the angle of attack oscillations caused by the initial conditions, vanish after about 8 s (Figs. 8a and 9a). In case 2, for the unstable parachute, the system continues to oscillate (Figs. 8b and 9b). When the parachute does not rotate the oscillation amplitude stays as large as 6.5 deg about an average of 19 deg (Fig. 8b), whereas for a rotating parachute the oscillation amplitude becomes much smaller with 2.5 deg about an average of 30 deg (Fig. 9b).

Figure 10 shows in more detail that the steady state values of α_L and α_P increase with angular rate $\boldsymbol{\Omega}_L$. From this can be concluded that the inclination angle of the symmetrical cylinder also increases with its angular rate. For the unstable parachute (Fig. 10b) a strong roll/yaw coupling is observed at $\boldsymbol{\Omega}_L = 1.6$ rev/s. Above this critical frequency the oscillation amplitude first decreases and then increases again.

Wind tunnel measurements[2,3] showed that the aerodynamic coefficients of parachutes can contain relatively large variations about their average values. Therefore, a stochastic dis-

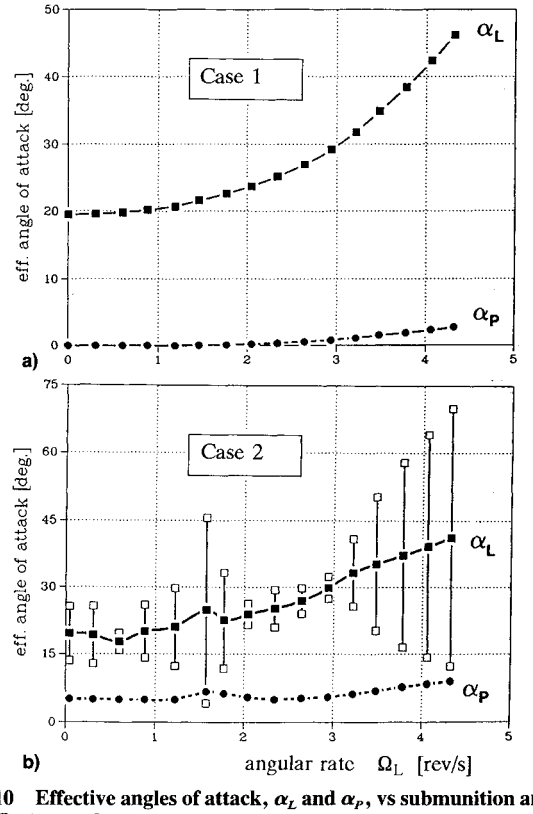

Fig. 10 Effective angles of attack, α_L and α_P, vs submunition angular rate $\boldsymbol{\Omega}_L$ in steady descent: a) case 1 (stable parachute), and b) case 2 (unstable parachute).

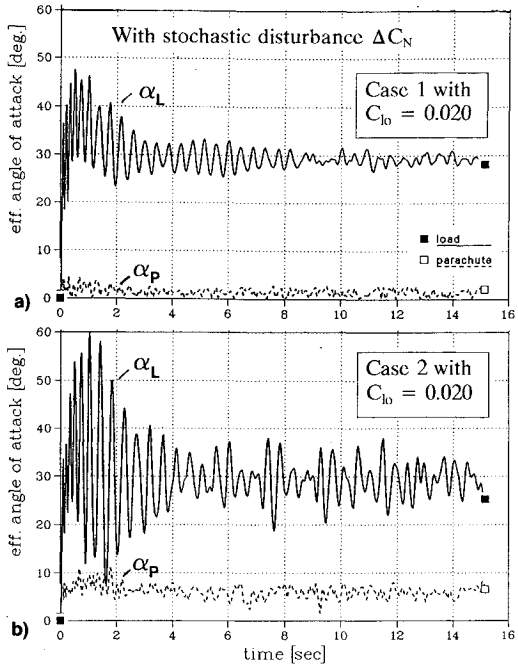

Fig. 11 Influence of parachute stochastic normal force variation ΔC_N on the effective angles of attack, α_L and α_P: a) case 1 (stable parachute), and b) case 2 (unstable parachute).

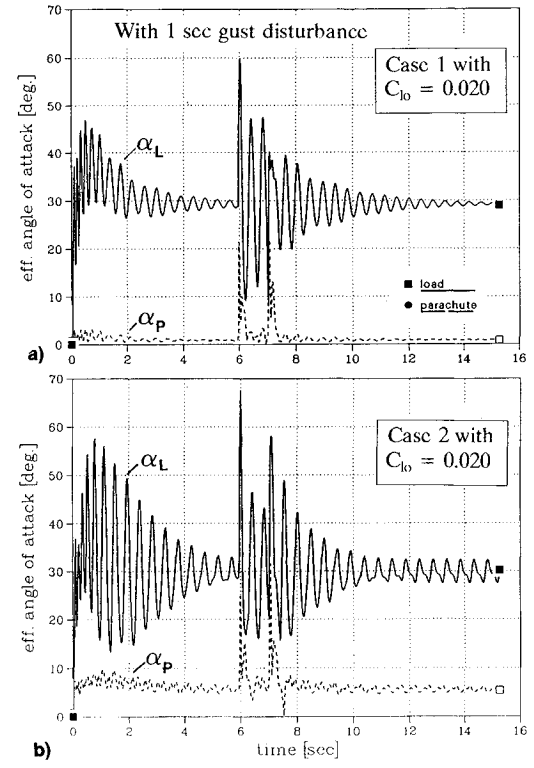

Fig. 12 Influence of a wind gust on the effective angles of attack, α_L and α_P: a) case 1 (stable parachute), and b) case 2 (unstable parachute).

turbance $\Delta C_N(t)$

$$\Delta C_N(t) = 0.02R(t) \tag{24}$$

has been added to the normal force coefficient $C_N(\alpha)$, where $R(t)$ is a random number between -1 and $+1$. For the stable parachute in case 1 this random input has only a small influence (Fig. 11a), but it more than doubles the oscillation amplitude for the unstable parachute in case 2 (Fig. 11b).

Finally, in Fig. 12 the effect of a 10 m/s horizontal wind gust of 1 s length is simulated. The gust causes large oscil-

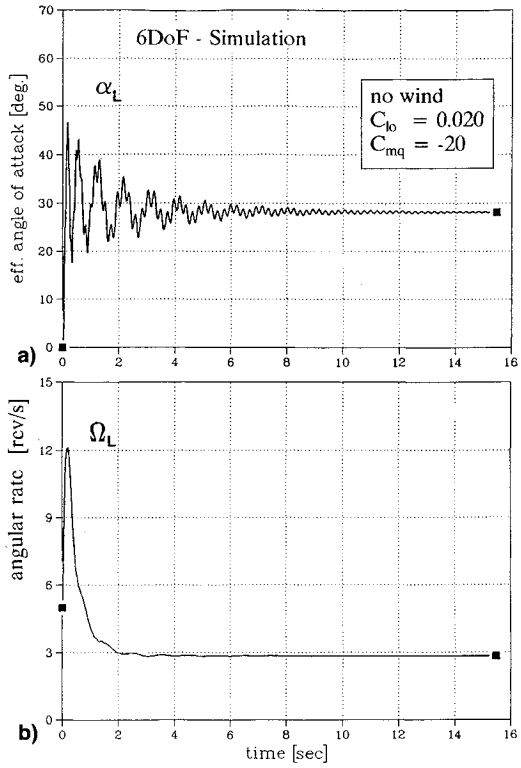

Fig. 13 6-DOF simulation with a massless parachute which produces only drag $C_{mq,L} = -20$, $C_{lo} = 0.020$; and no wind (corresponds to Figs. 7a and 9a).

lations which take many seconds to decay. This clearly demonstrates the sensitivity of the system to atmospheric disturbances and shows that there is very little damping of the pitch/yaw eigenmotion for the coupled parachute-load configuration.

D. Six-DOF Simulation

For comparison with the 9-DOF model, the results of a 6-DOF simulation are shown in Fig. 13. In the 6-DOF simulation a pitch damping coefficient of $C_{mq} = -20$ was assumed and the parachute was modeled only by a drag force. This corresponds to a very stable parachute as in case 1 in Fig. 9a. Accordingly, the angle-of-attack oscillation is quickly damped. This example indicates that 6-DOF simulations are not capable of predicting the dynamic behavior of rotating systems, when the parachute is not stable at $\alpha = 0$ deg. But this is precisely the situation, which often has to be anticipated in reality.

IV. Conclusions

Simulations with more than 6 DOF are necessary with an appropriate mathematical model of the joint between the load and the parachute in order to predict the dynamic behaviour of rotating parachute systems. Previous 6-DOF simulations have been overoptimistic in predicting the stability of such systems.

Rotating parachute systems are very sensitive to atmospheric disturbances. Any such disturbance results in oscillations of the load which can have considerable amplitudes. The required stable descent conditions can not be achieved with an unstable parachute.

References

[1]Wolf, D. F., "The Dynamic Stability of a Non-Rigid Parachute and Payload System," Ph.D. Dissertation, Univ. of Rhode Island, Kingston, RI, 1968.

[2]Doherr, K.-F., "Theoretical and Experimental Investigation of Parachute-Load-System Dynamic Stability," AIAA 5th Aerodynamic Deceleration Systems Conf., AIAA Paper 75-1397, Albu-

querque, NM, 17–19 Nov. 1975.

[3]Doherr, K.-F., "Theoretisch-experimentelle Untersuchung des dynamischen Verhaltens von Fallschirm-Last-Systemen bei Windkanalversuchen," Ph.D. Thesis, Technische Universität München, DFVLR-FB 81-29, Munich, 1981.

[4]Pillasch, D. W., Shen, Y. C., and Valero, N., "Parachute/Submunition System Coupled Dynamics," AIAA 8th Aerodynamic Decelerator and Balloon Technology Conf., AIAA Paper 84-0784CP, Hyannis, FL, 1984.

[5]Doherr, K.-F., and Saliaris, C., "Mathematisches Modell eines Fallschirm-Last-Systems," in CCG-UofM-Course F12.01 on "Parachute Systems Technology; Fundamentals, Concepts and Applications," Oberpfaffenhofen, June 22–26, 1987.

[6]Paus, M., "Entwicklung eines Simulationsprogramms zur Untersuchung freifliegender Fallschirm-Last-Systeme," Diplomarbeit, Techn. Univ. Braunschweig, Institut für Flugführung, Braunschweig, Nov. 1987.

[7]Robinson, A. C., "On the Use of Quaternions in Simulation of Rigid Body Motion," WADC TR 58-17, Dec. 1958.

[8]Doherr, K.-F., and Synofzik, R., "Investigations of Rotating Parachutes for Submunitions," AIAA 9th Aerodynamic Decelerator and Balloon Technology Conf., AIAA Paper 86-2438-CP, Albuquerque, NM, 7–9 Oct. 1986.

[9]Doherr, K.-F., and Cockrell, D. J., "Preliminary Consideration of Parameter Identification Analysis from Parachute Aerodynamic Test Data," AIAA 7th Aerodynamic Decelerator and Balloon Technology Conf., AIAA Paper 81-1940, San Diego, CA, Oct. 21–23, 1981.

[10]Yavuz, T., and Cockrell, D. J., "Experimental Determination of Parachute Apparent Mass and Its Significance in Predicting Dynamic Stability," AIAA 7th Aerodynamic Decelerator and Balloon Technology Conf., AIAA Paper 81-1920, San Diego, CA, Oct. 21–23, 1981.

[11]Cockrell, D. J., Doherr, K.-F., and Polpitiye, S. J., "Further Experimental Determination of Parachute Virtual Mass Coefficients," AIAA 8th Aerodynamic Decelerator and Balloon Technology Conf., AIAA Paper 84-0797-CP, Hyannis, FL, 1984.

[12]Cockrell, D. J., Shen, C. Q., Harwood, R. J., and Baxter, A. C., "Aerodynamic Forces Acting on Parachutes in Unsteady Motion and the Consequential Dynamic Stability Characteristics," AIAA 9th Aerodynamic Decelerator and Balloon Technology Conf., AIAA Paper 86-2470-CP, Albuquerque, NM, Oct. 7–9, 1986.